Journal of Solid State Chemistry 184 (2011) 546–556

Contents lists available at ScienceDirect

Journal of Solid State Chemistry

journal homepage: www.elsevier.com/locate/jssc

One-step synthesis and stabilization of gold nanoparticles and multilayer film assembly

Ya-Yan Bao, Li-Hua Bi *, Li-Xin Wu *

College of Chemistry, State Key Laboratory of Supramolecular Structure and Materials, Jilin University, Changchun 130012, People's Republic of China

ARTICLE INFO

Article history:
Received 19 August 2010
Received in revised form
24 December 2010
Accepted 10 January 2011
Available online 15 January 2011

Keywords:
Au nanoparticles
Tungstovanadate
Multilayer films
Layer-by-layer assembly
Electrocatalytic

ABSTRACT

Au nanoparticles (NPs) were synthesized in the one-pot procedure in water at room temperature with the wheel-shaped V^{V}–V^{IV} mixed-valence tungstovanadate $[P_8W_{48}O_{184}\{V^{V}_4V^{IV}_2O_{12}(H_2O)_2\}_2]^{32-}$ (V12) acting as both reducing and stabilizing agents. The V12 stabilized Au NPs (Au@V12 NPs) were characterized by SEM, TEM, DLS, UV–vis spectroscopy, XPS, and XRD analyses and the negatively charged surface of the Au@V12 NPs was proved by the zeta potential analysis. Based on the layer-by-layer assembly (LbL), the Au@V12 NPs-containing multilayer films have been fabricated on ITO-coated glass slide and quartz substrates with poly(ethyleneimine) (PEI). The regular growth of the multilayer films was monitored by UV–vis spectroscopy and cyclic voltammetry, the composition was characterized by XPS. The Au@V12 NPs based composite films showed electrocatalytic activities towards the reduction of dioxygen and the oxidation of methanol. This approach is expected to open the way towards procedures aimed at the one-step fabrication of Au NPs and polyoxometalates (POMs) into the multilayer films.

1. Introduction

Metal nanoparticles (NPs) have attracted increasing attention due to their fascinating optical and electrical properties, which are remarkably different compared with their bulk materials and are regulated by NPs size, shape, composition, aggregation state, and local surroundings [1–5]. Such unique properties make NPs promising candidates for the applications in the fields of optical, electronic, catalytic, sensing, biodiagnostics, materials science and so on [6–11]. In recent years, the studies on Au NPs have been widely developed including synthesis method and reaction condition [12], control of shape and size [13], selection of reaction reagents [14], etc. However, most Au NPs were prepared under an organic environment and a relatively high temperature in common. Thus, the further exploration of Au NPs synthesis under environmentally friendly conditions still remains a challenge.

Polyoxometalates (POMs) are exciting inorganic metal-oxygen cluster species with a diverse compositional range, enormous structural variety and interesting adjustable multi-functional properties, which have displayed reversible electron-transfer behaviors without any significant structural change [15]. Such reversible charge-transfer ability makes POMs ideal candidates for uniform-phase electron exchange process [16]. Based on such understanding, a new room temperature preparation method for Au NPs was developed, namely, POMs with partially reduced species were used both as reductants and stabilizers to synthesize Au NPs in water at room temperature. To date, of various Au nanostructures, such as spherical [17] or quasi-spherical NPs [18], triangular and hexagonal nanoplates, twisted nanowires [19], and flower-like NPs [20] were successfully synthesized via carefully selecting appropriate POMs and tuning the concentrations of the POMs or the molar ratio of metallic and POMs without any surfactant, seed or template. It can be seen that this strategy opens the promising way towards the "green-chemistry" synthesis of Au NPs via use of POMs. So far, several POMs have been used to synthesize Au NPs [21–24]. Usually, the selected POMs need to be firstly reduced by electrochemistry or photochemistry during the synthesis process of Au NPs. Here, we chose a wheel-shaped V^{V}–V^{IV} mixed-valence tungstovanadate $Na_{12}K_8H_4[K_8P_8W_{48}O_{184}\{V^{V}_4V^{IV}_2O_{12}(H_2O)_2\}_2]\cdot 80H_2O$ (V12) [25] with the reduction ability acting as both the reducing agent and the stabilizer to prepare Au NPs to simplify the synthesis process of Au NPs. In addition, the surface of the as-prepared Au NPs absorbed a layer of V12 polyanions, making the overall Au NPs negatively charged with a relatively hydrophilic surface, which was further fabricated into the multilayer films based on the electrostatic attraction with the positively charged poly(ethyleneimine) (PEI) by the layer-by-layer (LbL) assembly method.

In recent years, the LbL assembly method based on alternately electrostatic adsorption of oppositely charged species has been widely utilized to fabricate the multilayer films. More and more POMs with various structures have been incorporated into the

* Corresponding authors. Fax: +86 431 85193421.
E-mail address: blh@jlu.edu.cn (L.-H. Bi).

0022-4596/$ - see front matter © 2011 Elsevier Inc. All rights reserved.
doi:10.1016/j.jssc.2011.01.011

multilayer films by LbL method for developing the functional thin-film materials or devices. These composite films have displayed not only the electrocatalytic activities towards the reduction of substances such as NO, NO_2^-, NO_3^-, BrO_3^-, IO_3^-, H_2, and H_2O_2 [26–28] and the oxidation of substances including As_2O_3 and $C_2O_4^{2-}$ [29], but also the luminescence, electro-, and photo-chromic properties [30,31]. In addition, the potential application as pH-sensitive probe was reported [32]. Recently, the intense research has been devoted to the fabrication of POMs and NPs, including carbon nanotube [33], Pt NPs [39], Fe_3O_4 NPs [34], TiO_2 NPs [35], Bi_2O_3 NPs [36], and Ag NPs [37] to exhibit the synergistic properties originating from POMs and NPs. More recently, Liu and Tang prepared the photoswitchable fluorescence hybrid films based on photochromic POM $K_{14}[Na(H_2O)P_5W_{30}O_{110}]$ and luminescent core-shell CdSe@CdS NPs [38]. The above reports completely testified that POMs are ideal candidates to incorporate NPs into multidimensional arrays on the surface of different substrates. However to our knowledge, the exploration of POMs stabilized metallic NPs-based multilayer films as functional materials is relatively rare [39].

In this paper, we successfully prepared the V12 stabilized Au NPs (Au@V12 NPs) with the V^V–V^{IV} mixed-valence tungstovanadate $[P_8W_{48}O_{184}\{V_4^VV_2^{IV}O_{12}(H_2O)_2\}_2]^{32-}$ (V12, as shown in Fig. 1) acting as both reducing and stabilizing agents, and incorporated them into the multilayer films (as shown in Fig. 2) based on the following considerations: (i) Au NPs are synthesized in the one-pot procedure in water at room temperature with the selected POM. (ii) The stability of Au@V12 NPs is retained resulting from the existence of the repulsion forces of Au@V12 NPs with the negatively charged surface. (iii) The fabrication process of the multilayer films based on POMs and Au NPs is simplified, namely, Au NPs do not need to be synthesized alone. (iv) The positively charged species are easy to be incorporated into the Au@V12 NPs-based multilayer films by the LbL assembly method, which will open up the novel way towards the construction of the multifunctional thin-film materials or devices based on POMs, Au NPs, and functional positively charged species.

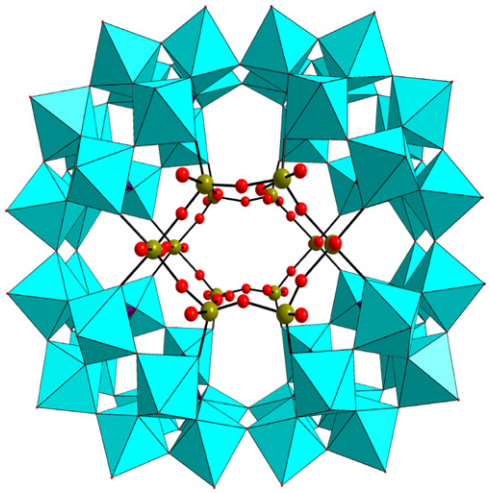

Fig. 1. Combined polyhedral/ball-and-stick representation of V12. Color code: V, dark yellow; O, red; WO_6, cyan; and PO_4, blue. (For interpretation of the references to colour in this figure, the reader is referred to the web version of this article.)

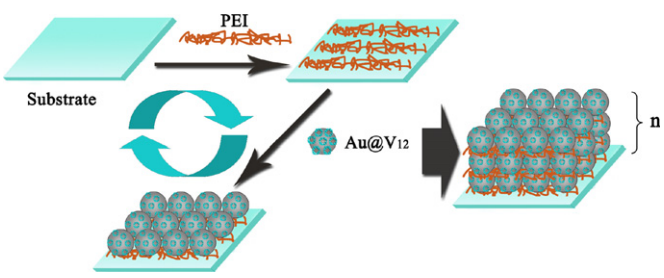

Fig. 2. Scheme of preparation of $(PEI/Au@V12)_n$ LbL multilayer films on the ITO-coated glass slides (not scaled).

2. Experimental section

2.1. Chemicals and methods

$Na_{12}K_8H_4[K_8P_8W_{48}O_{184}\{V_4^VV_2^{IV}O_{12}(H_2O)_2\}_2]\cdot 80H_2O$ (V12) was freshly prepared according to the literature procedure [25]. Poly(ethyleneimine) (PEI) was purchased from Aldrich and was used without further treatment. All of the other chemicals were of reagent grade and used as received unless stated. Ultrapure water (18 MΩ cm) delivered from a MilliPore system was employed in all experiments.

FT-IR spectra were carried out on a Bruker Vertex 80v FT-IR spectrometer equipped with a DTGS detector (32 scans) with a resolution of 4 cm^{-1} on a KBr pellet. X-ray photoelectron spectroscopy (XPS) spectra were acquired on an ESCALAB-250 spectrometer with a monochromic X-ray source (Al $K\alpha$ line, 1486.6 eV). Powder X-ray diffraction (XRD) data were recorded on a Rigaku X-ray diffractometer, using Cu $K\alpha$ radiation at a wavelength of 1.542 Å. Scanning electron microscope (SEM) images were obtained on a JEOL FESEM 6700F electron microscope, and transmission electron microscopic (TEM) images were carried out on a Hitachi H8100 electron microscope. Dynamic light scattering (DLS) was carried out on a DAWN Enhanced Optical System (DAWN EOS, Wyatt Technology Corporation). Zeta potential measurements were operated on a Nano-ZS instrument, model ZEN 3600 (Malvern Instruments). UV–vis absorption spectra were recorded out on a Shimadzu UV-3100 spectrometer, and the slit width was set at 2 nm. All electrochemical experiments were performed with CHI 660C electrochemical system at room temperature. A three-electrode electrochemical cell was used with an indium tin oxide (ITO)-coated glass slide as the working electrode, a platinum wire as counter electrode and Ag/AgCl as the reference electrode.

2.2. Preparation procedure of V12 stabilized Au NPs (Au@V12 NPs)

A series of concentrations 0.01, 0.05 and 0.1 mM of $HAuCl_4$ (Au acid) and 0.01, 0.05 and 0.1 mM of V12 solutions in water were prepared. The same amount (0.5 mL) of the above Au acid solutions were mixed with the corresponding concentrations of V12 solutions to prepare a series of reaction systems with same molar ratio of 1 from an Au acid to V12, which was defined as γ indicated by the following formulation: γ=[Au acid]/[V12], and different initial concentrations, namely, the Au acid and V12 concentrations ranged 0.01–0.1 mM. After mixing the two solutions for about 1 min or less the solution color turned from violet to orange, which indicated the reaction occurred quite quickly. The exact color nuance depended on the initial concentrations of Au acid and V12, suggesting the formation of different Au NPs, which was further demonstrated by UV–vis spectra.

The obtained suspension was sonicated for 30 min. Then, Au@V12 NPs were separated from the reaction mixture after centrifugation, washed with water, this procedure was typically repeated three or four times until the final suspension of Au NPs was permanently navy, and re-dispersed into water for analyses. It was worth noting that re-dispersion of the centrifuged Au NPs in water gave clear colloidal solutions, which could be remained stable for at least 1 month.

2.3. Preparation of the multilayer films containing Au@V12 NPs

A transparent ITO-coated glass slides or quartz substrates were treated according to the published procedure before use [40]. The freshly prepared slides were soaked for 20 min in an aqueous solution containing 7.0 wt% PEI, forming a precursor PEI layer with positively charged surface to which the negatively charged Au@V12 NPs could be adsorbed electrostatically. Then, the ITO/PEI slide was immersed in an Au@V12 NPs containing solution for 20 min. After thoroughly rinsing with water and drying with a nitrogen stream, the modified electrode with an Au@V12 NPs monolayer was transferred to the 7.0 wt% PEI solution again, resulting in the adsorption of another layer of PEI. When the resulting modified electrode was alternately placed in Au@V12 NPs and PEI solutions in a cyclic fashion, the Au@V12 NPs and PEI-containing multilayer films were formed. The thickness of the multilayer films was readily adjusted by choosing different numbers of cycles by the LbL modification method. The preparation of the multilayer films containing V12 was the same with that of Au@V12 NPs, except that the V12 solution was used instead of the Au@V12 NPs solution.

3. Results and discussion

3.1. Preparation of Au@V12 NPs

The precursor was $HAuCl_4$ (Au acid). The selected POM for this work was $Na_{12}K_8H_4[K_8P_8W_{48}O_{184}\{V^V_4V^{IV}_2O_{12}(H_2O)_2\}_2]\cdot 80H_2O$ (V12), which belongs to the wheel-shaped tungstovanadate containing two mixed-valence V6-type aggregate (see Fig. 1), namely, the reduced centers of V^{IV} are present in V12. In a typical experiment, a mixture containing 0.01, 0.05 and 0.1 mM Au acid and 0.01, 0.05 and 0.1 mM V12 was prepared, respectively, in water with $\gamma=1$, and then electron exchange reactions between Au acid and V12 took place automatically at room temperature without any additives, which displayed a quick color change of the solutions from violet to orange within 1 min, suggesting that the partial V^{IV} in V12 was converted to V^V continuously, accompanying the reduction of Au^{III}–Au^0. Because of the extremely low initial concentration of Au^0 in the solution, the typical dark blue color of an Au^0 could not be observed clearly in the mixture. However, dark blue precipitates could be obtained by separating from the orange solution after centrifugation, indicating the formation of Au NPs.

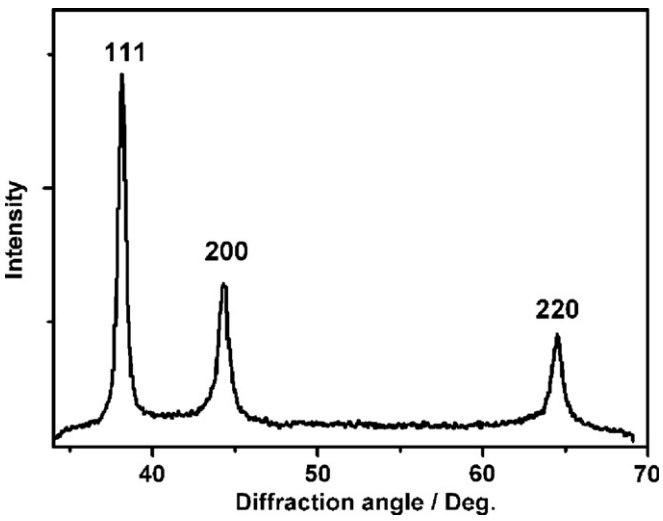

Fig. 3. Powder XRD pattern of the Au@V12 NPs with V12 initial concentration of 0.1 mM at $\gamma=1$.

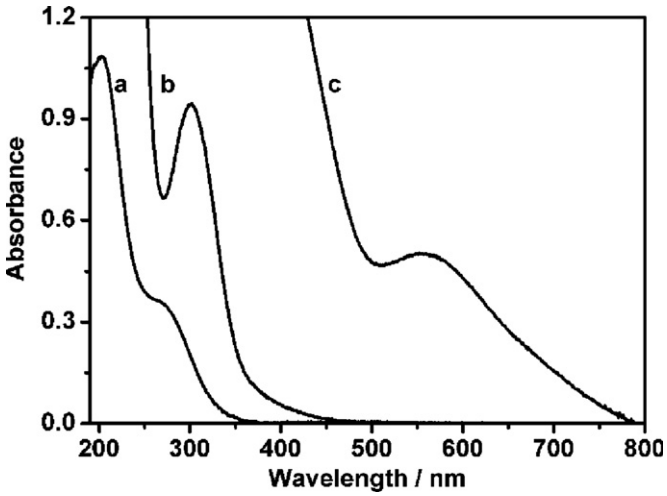

Fig. 4. Comparative UV–vis spectra of V12 (a), Au acid (b) and Au@V12 NPs (c) with [V12]=0.1 mM at $\gamma=1$.

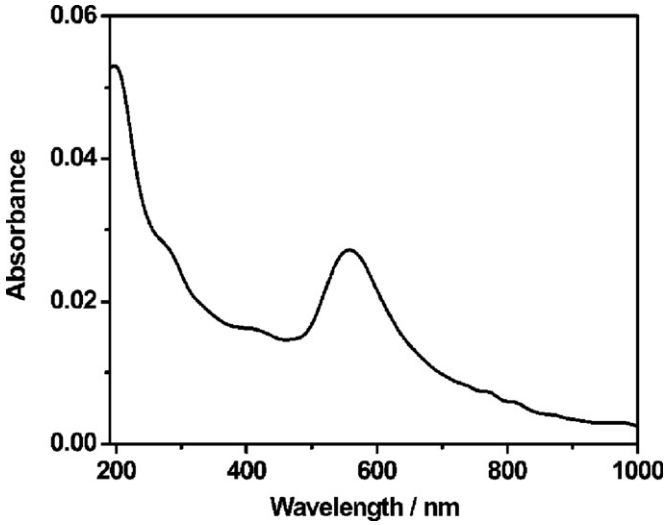

Fig. 5. UV–vis spectrum of Au@V12 NPs after centrifugation of the mixture with V12 original concentration of 0.1 mM at $\gamma=1$.

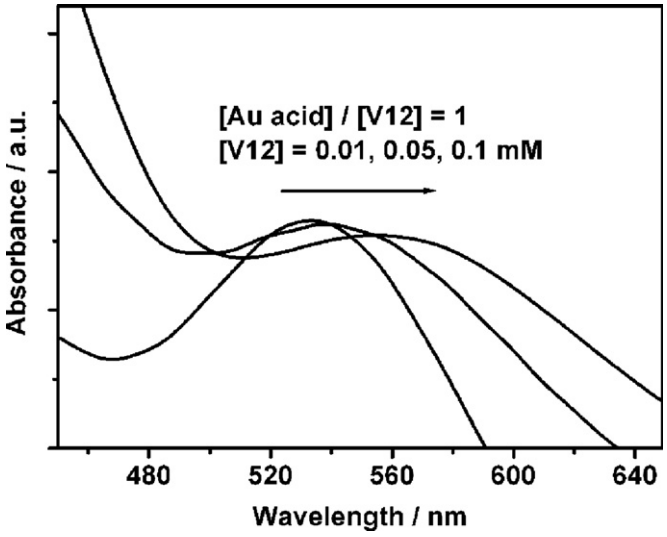

Fig. 6. UV–vis spectra of Au@V12 NPs with different V12 initial concentrations at $\gamma=1$.

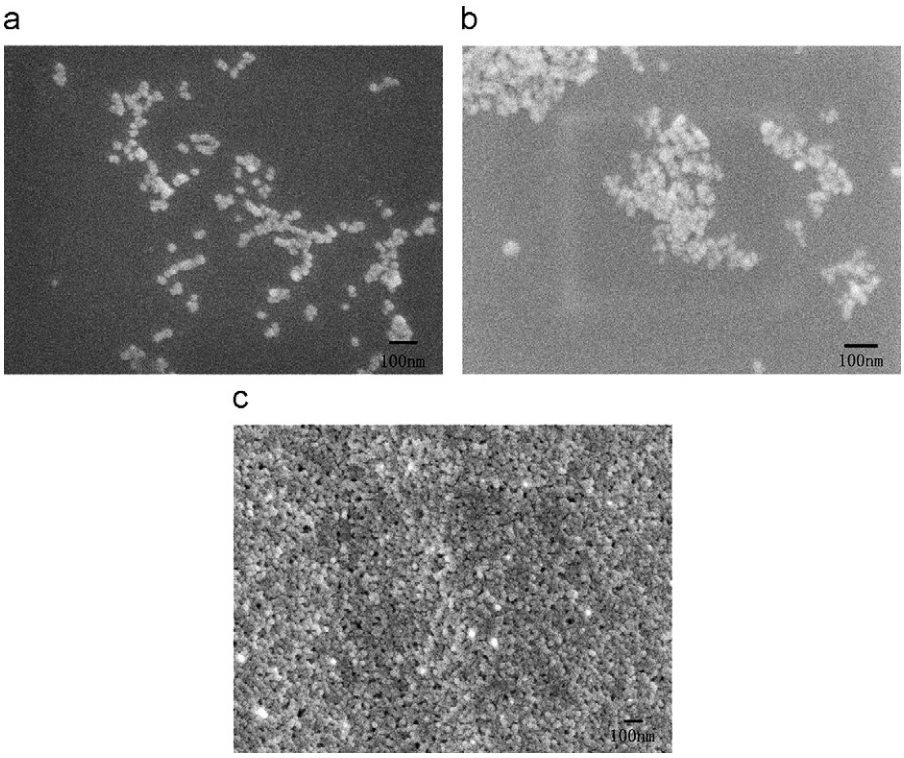

Fig. 7. SEM images of the Au@V12 NPs with different V12 initial concentrations of 0.01 (a), 0.05 (b) and 0.1 mM (c) at $\gamma=1$.

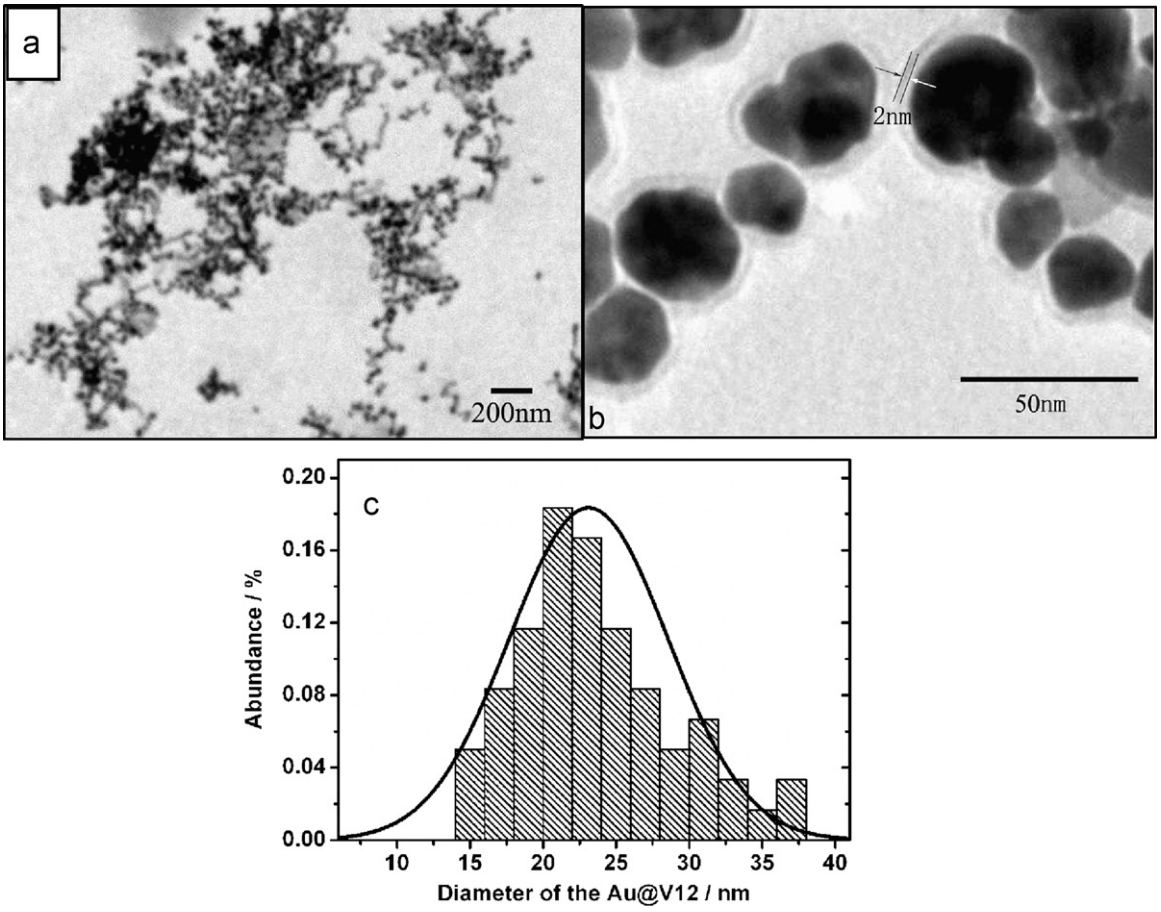

Fig. 8. (a) TEM image of the Au@V12 NPs with V12 initial concentration of 0.1 mM at $\gamma=1$; (b) a magnified TEM image of the Au@V12 NPs and (c) size histogram of Au@V12 NPs of about 60 NPs counted from the TEM image showing the distribution of Au@V12 NPs.

3.2. Characterization of Au@V12 NPs

3.2.1. Powder XRD pattern

Powder XRD analysis was performed to identify the crystal direction of the Au NPs. As shown in Fig. 3, the typical powder XRD pattern for Au@V12 NPs with the initial concentration of 0.1 mM at $\gamma=1$ clearly displayed the {1 1 1}, {2 0 0} and {2 2 0} Bragg reflections of face-centered cubic (fcc) of gold in agreement with the expectation of peaks at 38.1° {1 1 1}, 44.4° {2 0 0} and 64.7° {2 2 0} [41]. In addition, the intensity ratio of {1 1 1} to {2 0 0} diffraction peaks was larger than 1.9 of the standard diffraction of gold powders, suggesting that the nanocrystallites grow with the surfaces terminated by the lowest energy {1 1 1} facets [42]. An evaluation of the average diameter of Au NPs in the {1 1 1} direction through Scherrer formula applied to the {1 1 1} Bragg reflection gave a value of 23 ± 2 nm [43], in agreement with direct measurements from the TEM image.

3.2.2. UV–vis spectra

For comparison, the UV–vis spectra of V12 (curve *a*), Au acid (curve *b*) and Au@V12 NPs (curve *c*) with [V12]=0.1 mM at $\gamma=1$ in the solutions were shown in Fig. 4. The peak at *ca.* 558 nm in curve *c*, which was observed after mixing Au acid and V12 solutions, was featured for the Au NPs. For clarity, Au@V12 NPs were separated from the reaction mixture after centrifugation, washed with water, and re-dispersed in water, its UV–vis spectrum was shown in Fig. 5. In Fig. 5, a broad absorbance band at *ca.* 558 nm, featuring a typical dipole resonance associated with spherical or quasi-spherical Au NPs [44,45], was observed, which was indicative of the formation of Au NPs. In addition, peaks at *ca.* 200 and 270 nm for V12 were all found, indicating the formation of V12 stabilized Au NPs, Au@V12 NPs. When γ value was kept at 1 and concentrations of V12 and Au acid were varied from 0.01, 0.05–0.1 mM, the UV–vis peak location changes with the difference of the initial concentrations, as shown in Fig. 6. It could be concluded that increasing the initial concentrations of Au acid and V12 induces the red shifts of the UV–vis peaks of Au NPs. These observations displayed an influence of the initial concentrations on the formation of Au NPs, which were completely consistent with theoretical expectations based on the evolution of NPs size [44,46] and with experimental phenomena for similar systems [42,47].

3.2.3. SEM and TEM images

Fig. 7 is SEM images of the Au@V12 NPs with different initial concentrations of 0.01 (a), 0.05 (b), 0.1 mM (c) at $\gamma=1$. In full agreement with the UV–vis spectra, the NPs were spherically shaped with a diameter of around 30 nm and a scattered size distribution.

For TEM measurements, the sample drops were deposited and dried on a carbon-coated copper grid. A representative image is shown in Fig. 8a, obtained from the initial concentration of 0.1 mM with $\gamma=1$. The NPs were spherically shaped and quasi-monodisperse (standard deviation $<10\%$) with a diameter around 23 nm, in agreement with the histogram of about 60 NPs counted from the TEM image (Fig. 8c).

The obtained colloidal solution was very stable and did not show any precipitate at least 1 month without adding any organic stabilizer, implying that the V12 served both as a reductant and an efficient stabilizer. TEM observations further demonstrated

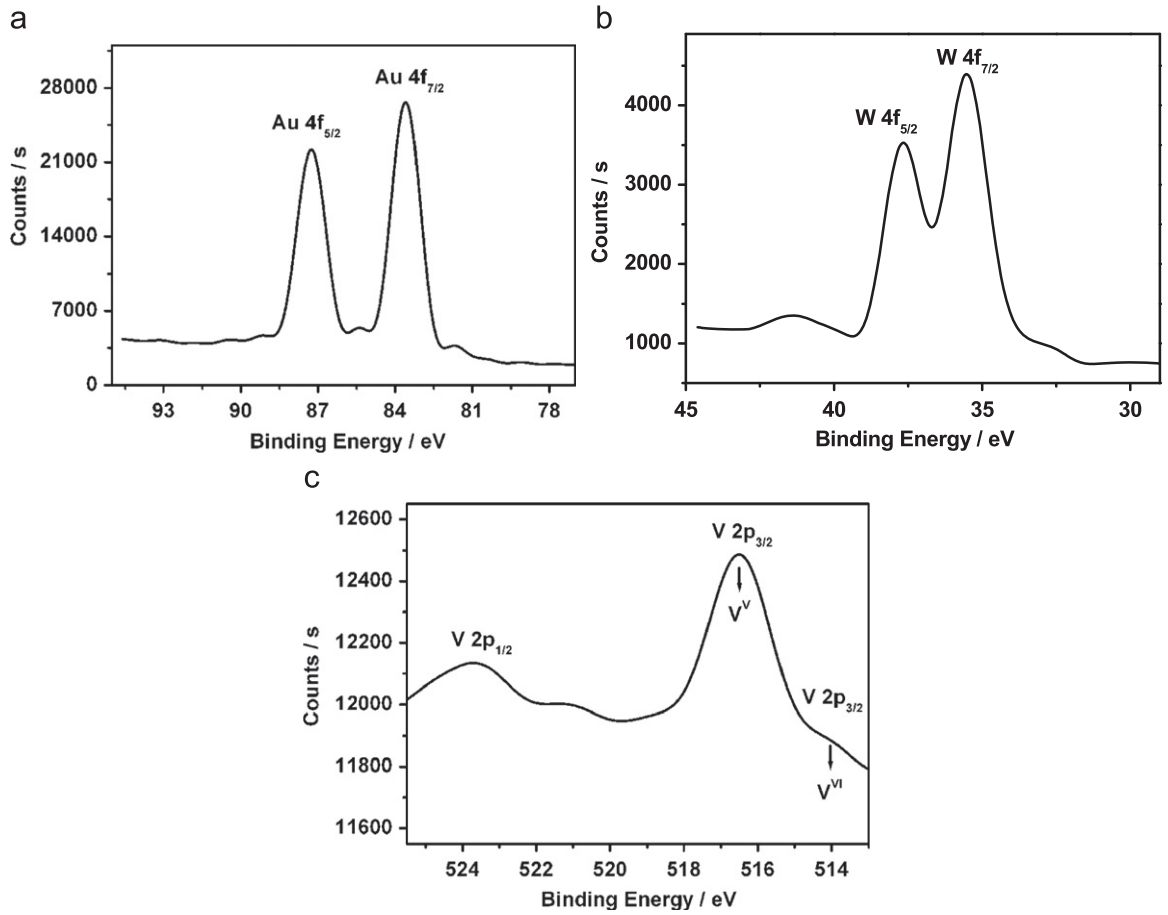

Fig. 9. XPS spectra of the Au@V12 NPs with (a) Au 4f; (b) W 4f and (c) V 2p with an initial concentration of 0.1 mM at $\gamma=1$.

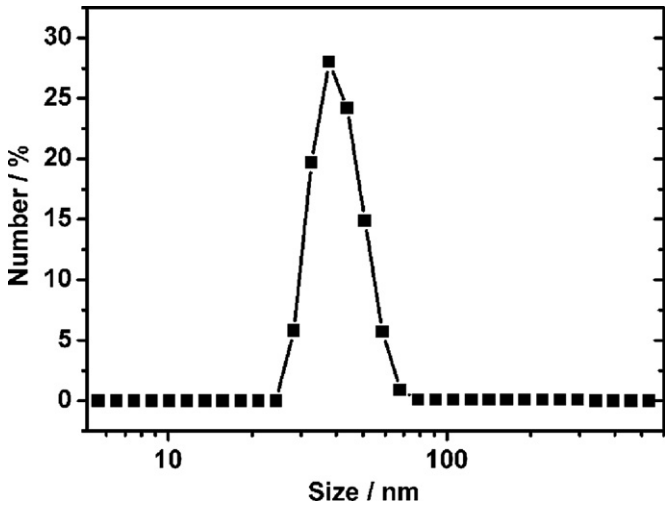

Fig. 10. DLS curve of the Au@V12 NPs with V12 initial concentration of 0.1 mM at $\gamma=1$ in water.

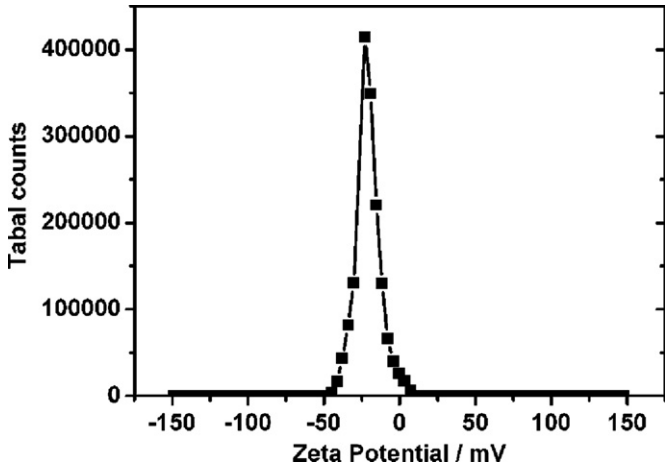

Fig. 11. Zeta potential pattern of the Au@V12 NPs with the V12 initial concentration of 0.1 mM at $\gamma=1$ in water.

a core-shell structure of Au@V12 NPs. After the TEM image of the same sample was magnified than that in Fig. 8a, a thin layer thickness with around 2 nm was clearly observed in Fig. 8b, which displayed the same size with that of V12. Such core-shell structure was always observed for POM stabilized NPs [20,48]. In addition, XPS analyses further supported such core-shell structure of Au@V12 NPs.

3.2.4. XPS measurements

The sample for the XPS analysis was deposited on the silicon substrate as supports. The analysis was carried out on Au@V12 NPs with the initial concentration of 0.1 mM at $\gamma=1$. As shown in Fig. 9a, typical XPS results gave the characteristic Au 4f peaks in two valence states: Au^0 (located at 83.6 and 87.3 eV for $4f_{7/2}$ and $4f_{5/2}$ levels, respectively) and Au^{III} (85.4 and 89.2 eV for $4f_{7/2}$ and $4f_{5/2}$ levels, respectively). However, the amount of Au^{III} was very low and the amount of Au^0 was the most abundant species in the mixture, thus confirming the effectiveness of the reduction process. In addition, it can be seen from Fig. 9b and c, two characteristic W 4f peaks (35.6 and 37.6 eV) and three V 2p peaks (514.3, 516.5 and 523.7 eV) were also observed, respectively, despite the sample has been washed thoroughly. These observations supported our proposal that the V12 served both as a reductant and as a capping layer. Similar cases have been found for POMs stabilized metal NPs [20].

3.2.5. DLS analysis

In order to measure the distribution of Au@V12 NPs in water, the DLS analysis was performed. It was indicated in Fig. 10 that the aggregates had a hydrodynamic radius (Rh) centered at 37.8 nm. From repeated experiments, we found that the aggregates of Au@V12 NPs were quite stable, because both the scattering intensity and Rh change little even upon standing at room temperature for more than one month. The size given by SEM, TEM and powder XRD was smaller than the result of DLS, but this was understandable due to the drying-induced shrinkage [49].

3.2.6. Zeta potential analysis

We employed the zeta potential technique to measure the surface potential of Au@V12 NPs being at −24.6 mV, as shown in Fig. 11, which indicated that the surface of Au@V12 NPs in water is negatively charged. It was apparent that the V12 polyanions were adsorbed on the surface of Au NPs, resulting in the formation of

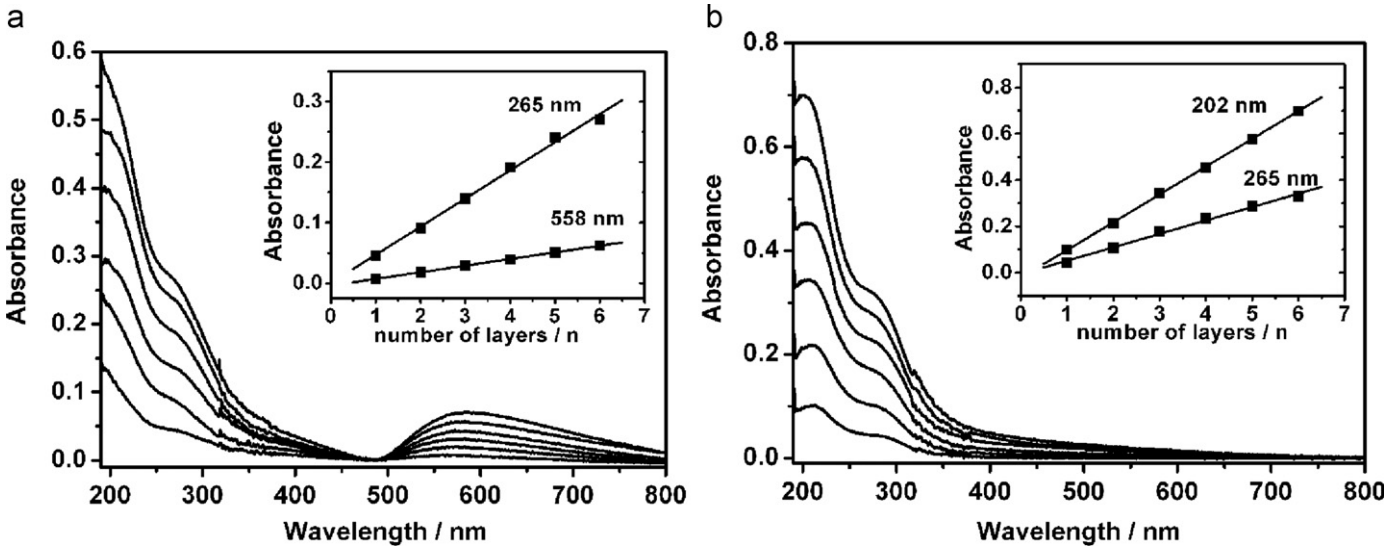

Fig. 12. UV–vis absorption spectra of the multilayer films of (a) $\{PEI/Au@V12\}_6$ and (b) $\{PEI/V12\}_6$ on the quartz substrates with an increase of the number of layers from 1 to 6 (from bottom to top). The insets show the relationships of the absorbencies versus the layer number of the multilayer films.

core-shell Au@V12 NPs; therefore, this observation inspired us to further fabricate Au@V12 NPs into the multilayer films based on alternately electrostatic adsorption of oppositely charged species by the LbL method.

3.3. Characterization of the multilayer films

3.3.1. UV–vis absorption spectra

UV–vis absorption spectra were applied to monitor the fabrication process of the multilayer films. For comparison, two films containing Au@V12 NPs and V12 were prepared simultaneously at the same experimental conditions. Fig. 12 depicts the UV–vis absorption spectra of two films containing six layers of $\{PEI/Au@V12\}_6$ or $\{PEI/V12\}_6$ deposited onto quartz substrates. Compared with the UV–vis absorption bands of V12 in water at *ca.* 265 nm, which were derived from the intramolecular charge transition of V12, the absorption bands of two films both exhibited a slight shift (from 265 to 268 nm for the $\{PEI/Au@V12\}_6$ film and from 265 to 271 nm for the $\{PEI/V12\}_6$ film), indicating similar electronic structure of V12 in two films. The different red shift of the absorption band should be attributed to the electrostatic interaction of V12 with PEI

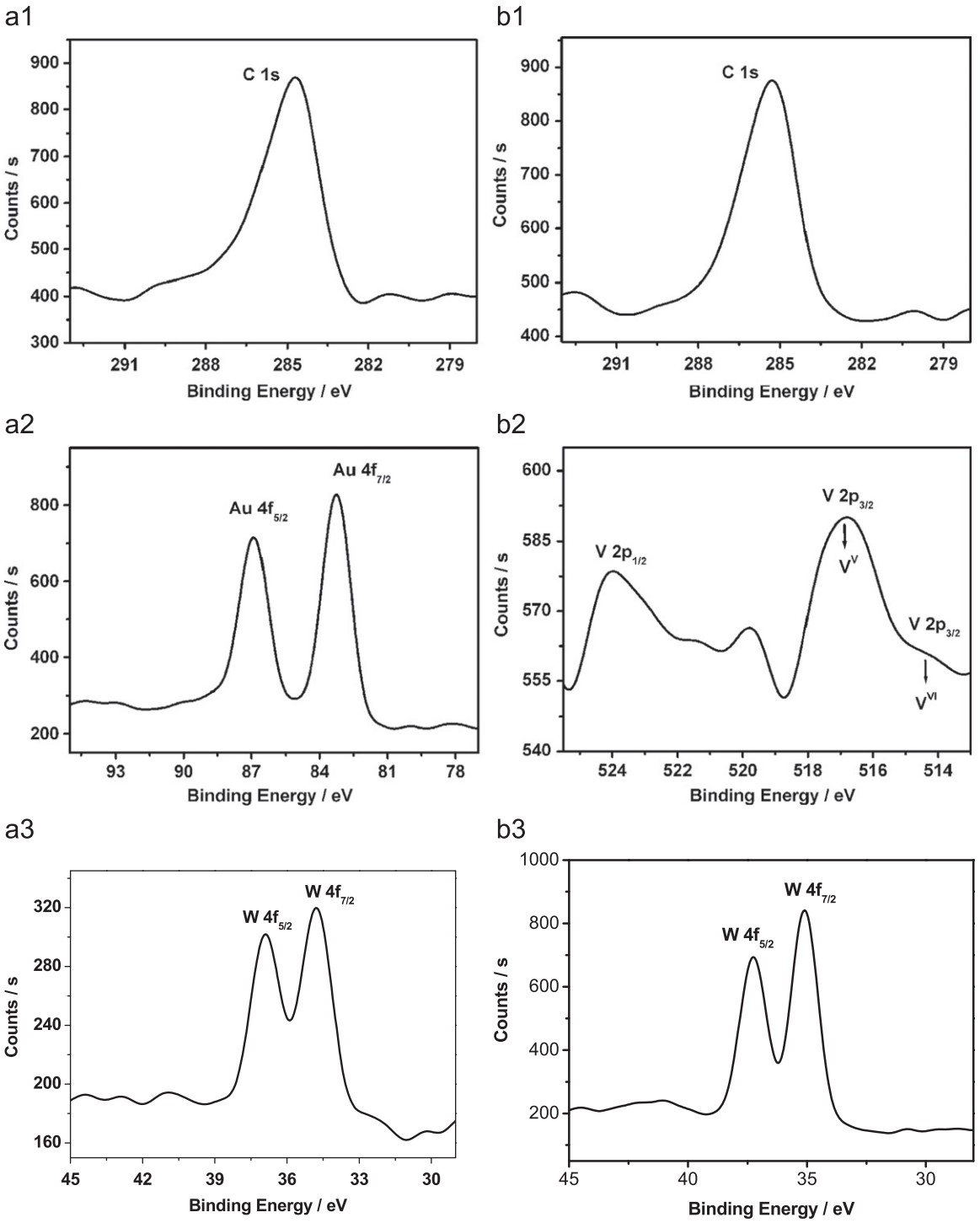

Fig. 13. XPS spectra for (a1) carbon, (a2) gold and (a3) tungsten of $\{PEI/Au@V12\}_7$ film; and for (b1) carbon, (b2) vanadium and (b3) tungsten of the $\{PEI/V12\}_{20}$ film.

and the different environments around V12, which have been observed in many films containing POMs [50].

In addition, for comparison, 265 and 558 nm for $\{PEI/Au@V12\}_6$ film and 202 and 265 nm for $\{PEI/V12\}_6$ film were chosen, respectively, as the characteristic bands. As shown in insets in Fig. 12, there are obvious linear relationships of the absorbencies of characteristic bands versus the number of layers, indicating the stable, uniform deposition in each dipping cycle for two films.

3.3.2. XPS measurements

XPS measurements were conducted to identify the elements presented in the multilayer films of $\{PEI/Au@V12\}_7$ and $\{PEI/V12\}_{20}$. As shown in Fig. 13, for $\{PEI/Au@V12\}_7$ film two characteristic peaks of Au^0 4f (83.25 eV (7/2) and 86.9 eV (5/2)), C1s (284.7) and W 4f (34.8 eV (7/2) and 36.9 eV (5/2)) were observed, respectively; for $\{PEI/V12\}_{20}$ film, the characteristic peaks of V 2p (514.4 V^{IV} (3/2), 516.8 (V^V, 3/2) and 523.7 eV (V^V, 1/2)), C1s (285.3 eV) and W 4f (35.3 eV (7/2) and 37.4 eV (5/2)) were found, respectively. These XPS results further demonstrated that the presence of Au@V12 NPs, V12 and PEI in the multilayer films.

3.3.3. AFM measurements

AFM has been often used as an important tool for studying the multilayer films to provide further detailed information involving the surface morphology and homogeneity of the multilayer films. Fig. 14 displays AFM images of the multilayer films of $\{PEI/Au@V12\}_6$ (see Fig. 14a) and $\{PEI/V12\}_6$ (see Fig. 14b) prepared at the same experiment conditions with Au@V12 NPs and V12 as the outermost layer, respectively. It could be clearly seen that two multilayer films both exhibited the formation of numerous domains with some roughness. These domains were considered as the aggregation of Au@V12 NPs and V12 polyanions on the surface of the multilayer films.

Based on the AFM image of the multilayer films $\{PEI/Au@V12\}_6$, the multilayer films containing Au@V12 NPs showed the surface height of *ca.* 20 nm and the size of nanoclusters diameter of *ca.* 150–300 nm with the average surface roughness (*Ra*) of 53.35 nm and the largest roughness (*Rz*) of 119.90 nm. In comparison, according to the AFM image of the multilayer films $\{PEI/V12\}_6$, the multilayer films containing V12 showed the surface height of *ca.* 10 nm and the size of nanoclusters diameter of *ca.*100–200 nm with the average surface roughness (*Ra*) of 28.00 nm and the largest roughness (*Rz*) of 73.23 nm. The comparison of the AFM images of two multilayer films indicated that the surface morphology of the multilayer films $\{PEI/Au@V12\}_6$ was significantly different from that of the multilayer films $\{PEI/V12\}_6$, namely, the surface of $\{PEI/Au@V12\}_6$ film was rougher than that of the $\{PEI/V12\}_6$ film. We thus conjectured that Au@V12 NPs could not be closely packed on the multilayer films, because V12 polyanions were distributed around the Au NPs to form Au@V12 NPs, resulting in the larger size of Au@V12 NPs than that of V12.

3.3.4. Electrochemical behaviors of the multilayer films

The LbL assembly method based on the electrostatic attraction between PEI and Au@V12 NPs or V12 was used to build up the multilayer films by alternately dipping ITO-coated glass slide in PEI and Au@V12 or V12 solutions, respectively. After each modification, cyclic voltammetry was employed to characterize the increase in quantity of modifiers loaded in the multilayer films. Fig. 15 shows the cyclic voltammograms (CVs) in pH 3 buffer solutions (0.5 M Na_2SO_4+H_2SO_4) in the potential region of 1.0 to −0.6 V for ITO/$\{PEI/Au@V12\}_5$ multilayer films with Au@V12 as the outmost layer and of 1.0 to −0.9 V for ITO/$\{PEI/V12\}_5$ multilayer films with V12 as the outmost layer at different layer numbers of 1–5, respectively. It can be seen in Fig. 15 that the peak currents increased with the increase of the number of $\{PEI/Au@V12\}_n$ and $\{PEI/V12\}_n$ layers. For ITO/$\{PEI/Au@V12\}_5$ multilayer films, taking the first oxidation peak of the W centers as representative, the oxidation peak current had a good linear relationship with the number of layers, as shown in the inset of Fig. 15a. For ITO/$\{PEI/V12\}_5$ multilayer films, taking the second redox peak of the W centers as representative, the redox peak current showed a good linear relationship with the number of layers, as shown in the inset of Fig. 15b. The above results confirmed that the homogeneous multilayer films containing Au@V12 or V12 have been fabricated on ITO-coated glass slides.

3.3.5. Electrocatalytic activities of the multilayer films on the reduction of dioxygen and the oxidation of methanol

The catalytic activities for the reduction of dioxygen and the oxidation of methanol at Au@V12 NPs and V12 modified ITO-coated glass electrodes were studied. As shown in Fig. 16a,

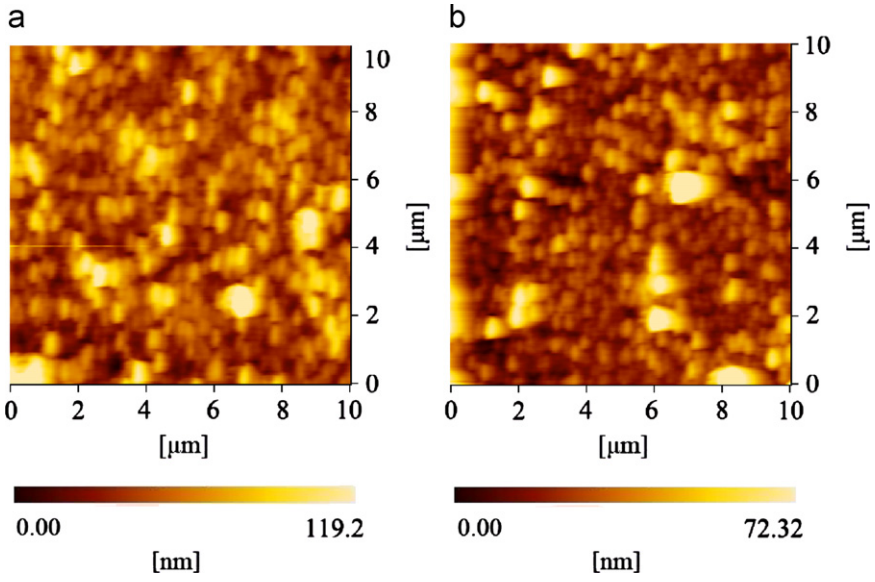

Fig. 14. AFM images of the multilayer films of (a) $\{PEI/Au@V12\}_6$ with Au@V12 NPs as the outmost layer and (b) $\{PEI/V12\}_6$ with V12 as the outermost layer.

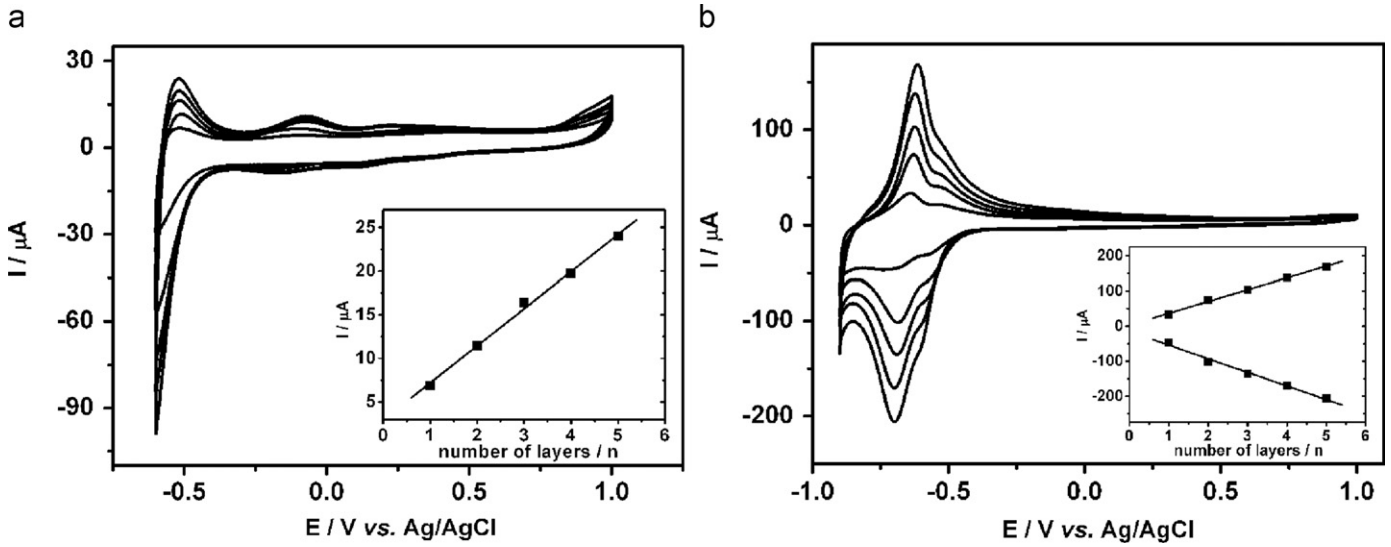

Fig. 15. (a) CVs of $\{PEI/Au@V12\}_n$ multilayer films with $n=1$–5 (from inside to outside) on an ITO-coated glass slide; (inset) linear dependence of the anodic peak currents with the number of layers. (b) CVs of $\{PEI/V12\}_n$ multilayer films with $n=1$–5 (from inside to outside) on an ITO-coated glass slide; (inset) linear dependence of the redox peak currents with the number of layers. Supporting electrolyte: 0.5 M Na_2SO_4+H_2SO_4, pH=3, scan rate: 20 mV s^{-1}.

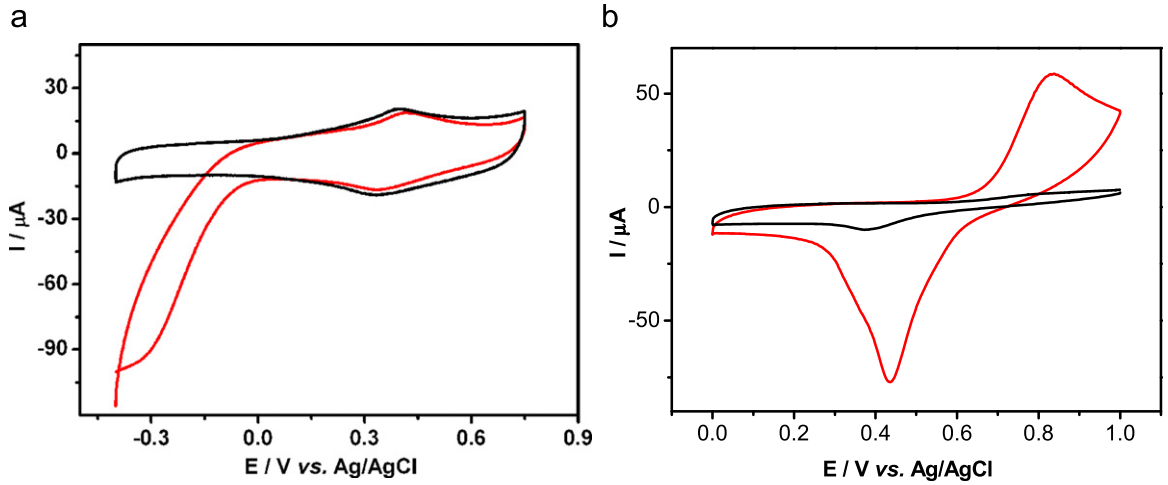

Fig. 16. CVs of the multilayer films of $\{PEI/Au@V12\}_6$ on an ITO-coated glass slide (a) in 0.5 M Na_2SO_4+H_2SO_4 buffer solution (pH 3) in the absence (black) and presence (red) of O_2; (b) in 1 M KCl solution (pH 7) in the absence (black) and presence (red) of methanol. Scan rate: 20 mV s^{-1}. (For interpretation of the references to colour in this figure, the reader is referred to the web version of this article.)

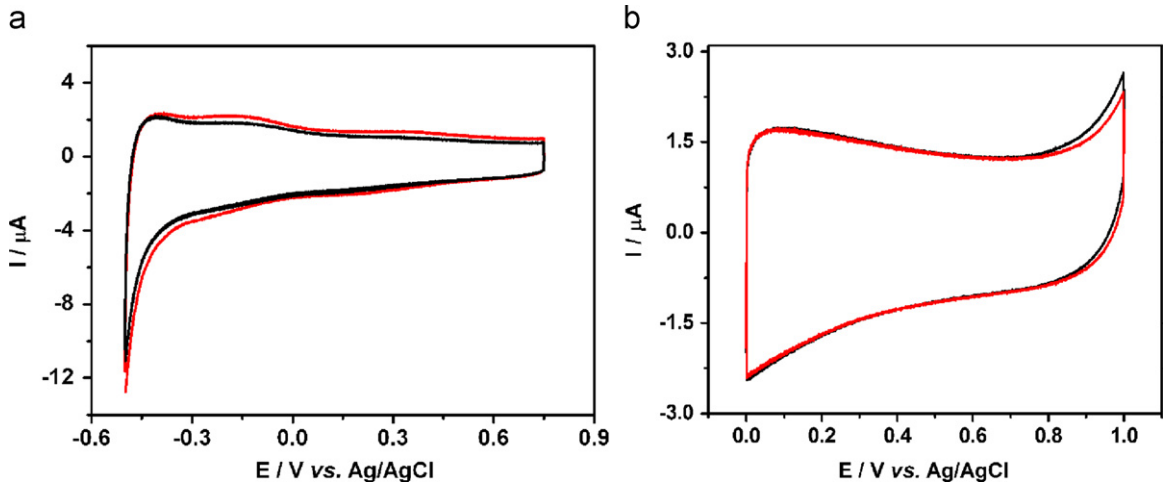

Fig. 17. CVs of the multilayer films of $\{PEI/V12\}_6$ on an ITO-coated glass slide (a) in 0.5 M Na_2SO_4+H_2SO_4 buffer solution (pH 3) in the absence (black) and presence (red) of O_2; (b) in 1 M KCl solution (pH 7) in the absence (black) and presence (red) of methanol. Scan rate: 20 mV s^{-1}. (For interpretation of the references to colour in this figure legend, the reader is referred to the web version of this article.)

the red curve is the CV for dioxygen reduction in air-saturated pH 3 buffer solution (0.5 M Na_2SO_4+H_2SO_4) at the ITO/$\{PEI/Au@V12\}_6$ electrode, and the black curve was obtained in an N_2-saturated solution. It can be seen from Fig. 16a, a marked catalytic reduction current occurred at the $\{PEI/Au@V12\}_6$ multilayer films at -0.3 V, however, same case could not be observed at the $\{PEI/V12\}_6$ multilayer films adsorbed on an ITO-coated glass electrode (see Fig. 17a) at the same experiment conditions, suggesting that the Au@V12 NPs modified electrode had high catalytic activity for the dioxygen reduction.

In addition, the Au@V12 NPs modified electrode also exhibited an electrocatalytic activity towards the oxidation of methanol in pH 7.0 KCl solution, as shown in Fig. 16b. It was clear that the anodic current becomes substantially increased on the addition of methanol. Apparently, the $\{PEI/Au@V12\}_6$ multilayer films can catalyze the electrochemical oxidation of methanol; in contrast, the $\{PEI/V12\}_6$ multilayer films did not show any catalytic activity for the oxidation of methanol at the same experiment conditions (see Fig. 17b).

4. Conclusions

In summary, we have prepared Au@V12 NPs by the redox reaction of Au acid and V12 in water at room temperature without any catalyst and selective etching agent, in which the V12 acted as reductant and stabilizer. Such Au@V12 NPs displayed the negatively charged surface, which was proved by the zeta potential analysis. Based on the LbL assembly, the Au@V12 NPs have been successfully incorporated into the multilayer films of $\{PEI/Au@V12\}_n$ on the substrates. For comparison, the multilayer films of $\{PEI/V12\}_n$ were also prepared. The results indicated the multilayer films of $\{PEI/Au@V12\}_6$ possessed good electrocatalytic activities toward the reduction of dioxygen and the oxidation of methanol, while the multilayer films of $\{PEI/V12\}_6$ did not work at the same experiment conditions. This study presented here should be applicable to an extended combination of functionalized metallic NPs and functional species for the fabrication of the multifunctional thin-film materials. It is believed that such hybrid thin-film systems may find potential applications in nanotechnology and material science.

Acknowledgments

The authors thank the financial support from the National Basic Research Program of China (2007CB808003), the National Natural Science Foundation of China (21073076), the Science Foundation of Jilin University, the Technology of Jilin Province, China (20090592) and the Open Projects of State Key Laboratory of Electroanalytical Chemistry of the Chinese Academy of Sciences (SKLEAC2010002), CAS.

Appendix A. Supplementary materials

Supplementary material associated with this article can be found in the online version at doi:10.1016/j.jssc.2011.01.011.

References

[1] S.Q. Liu, Z.Y. Tang, J. Mater. Chem. 20 (2010) 24.
[2] K. Revital, L. Michal, M. Leila, V. Maida, P. Ronit, A.I. Mark, E.B. Milko, Angew. Chem. Int. Ed. 49 (2010) 1218.
[3] Y. Cui, Q.Q. Wei, H.K. Park, C.M. Lieber, Science 293 (2001) 1289.
[4] M. Bockrath, W.J. Liang, D. Bozovic, J.H. Hafner, C.M. Lieber, M. Tinkham, H.K. Park, Science 291 (2001) 283.
[5] (a) Y.G. Jiang, Z.Q. Wang, X. Yu, F. Shi, H.P. Xu, X. Zhang, M. Smet, W. Dehaen, Langmuir 21 (2005) 1986;
(b) S.J. Guo, E.K. Wang, Anal. Chim. Acta 598 (2007) 181.
[6] L. Zhong, T.F. Hao, M.H. Liu, Langmuir 24 (2008) 11677.
[7] A. Naushad, A.M. Maqsood, F.M. Al-Nowaiser, K. Zaheer, Colloids Surf. B. 78 (2010) 109.
[8] S.J. Guo, S.J. Dong, E.K. Wang, Adv. Mater. 22 (2010) 1269.
[9] S.J. Guo, S.J. Dong, E.K. Wang, Chem. Commun. 46 (2010) 1869.
[10] N.L. Rosi, C.A. Mirkin, Chem. Rev. 105 (2005) 1547.
[11] C.A. Mirkin, R.L. Letsinger, R.C. Mucic, J.J. Storhoff, Nature 382 (1996) 607.
[12] (a) B.L. Cushing, V.L. Kolesnichenko, C.J. O'Connor, Chem. Rev. 104 (2004) 3893;
(b) J.L. Gu, W. Fan, A. Shimojima, T. Okubo, J. Solid State Chem. 181 (2008) 957.
[13] (a) Y.Y. Zhao, W. Qi, W. Li, L.X. Wu, Langmuir 26 (2010) 4437;
(b) C.X. Kan, C.S. Wang, J.J. Zhu, H.C. Li, J. Solid State Chem. 183 (2010) 858.
[14] Y. Zheng, P.D. Stevens, Y. Gao, J. Am. Chem. Soc. 123 (2001) 5743.
[15] (a) P.T. Ma, J.W. Zhao, J.P. Wang, Y. Shen, J.Y. Niu, J. Solid State Chem. 183 (2010) 150;
(b) S.T. Zhen, G.Y. Yang, Dalton Trans. 39 (2010) 700;
(c) J. Zhang, J. Hao, Y.G. Wei, F.P. Xiao, P.C. Yin, L.S. Wang, J. Am. Chem. Soc. 132 (2010) 14;
(d) C. Jahier, S.S. Mal, U. Kortz, S. Nlate, Eur. J. Inorg. Chem. (2010) 1559;
(e) J. Zhang, D. Li, G. Liu, K.J. Glover, T.B. Liu, J. Am. Chem. Soc. 131 (2009) 15152;
(f) J. Zhang, B. Keita, L. Nadjo, I.M. Mbomekalle, T.B. Liu, Langmuir 24 (2008) 5277.
[16] A. Dolbecq, J.D. Compain, P. Mialane, J. Marrot, F. Secheresse, B. Keita, L.R.B. Holzle, F. Miserque, L. Nadjo, Chem. A—Eur. J. 15 (2009) 733.
[17] B. Keita, R.N. Biboum, I.M. Mbomekalle, S. Floquet, C. Simonnet-Jégat, E. Cadot, F. Miserque, P. Berthet, L. Nadjo, J. Mater. Chem. 18 (2008) 3196.
[18] A. Troupis, A. Hiskia, E. Papaconstantinou, Angew. Chem. Int. Ed. 41 (2002) 1911.
[19] G.J. Zhang, B. Keita, R.N. Biboum, F. Miserque, P. Berthet, A. Dolbecq, P. Mialane, L. Catala, L. Nadjo, J. Mater. Chem. 19 (2009) 8639.
[20] H.L. Li, Y. Yang, Y.Z. Wang, W. Li, L.H. Bi, L.X. Wu, Chem. Commun. 46 (2010) 3750.
[21] S. Mandal, A. Das, R. Srlvastava, M. Sastry, Langmuir 21 (2005) 2408.
[22] A. Troupis, A. Hiskia, E. Papaconstantinou, Appl. Catal. B. 52 (2004) 41.
[23] S. Mandal, P.R. Selvakannan, R. Parischa, M. Sastry, J. Am. Chem. Soc. 125 (2003) 8440.
[24] T. Kida, R. Oshima, K. Nonaka, K. Shimanoe, M. Nagano, J. Phys. Chem. C. 113 (2009) 19986.
[25] A. Müller, M.T. Pope, A.M. Todea, H. Bogge, J. van Slageren, M. Dressel, P. Gouzerh, R. Thouvenot, B. Tsukerblat, A. Bell, Angew. Chem. Int. Ed. 46 (2007) 4477.
[26] L.H. Bi, T. McCormac, S. Beloshapkin, E. Dempsey, Electroanalysis 20 (2008) 38.
[27] B. Keita, P. Mialane, F. Secheresse, P. de Oliveira, L. Nadjo, Electrochem. Commun. 9 (2007) 164.
[28] H.Y. Ma, T. Dong, G. Wang, W. Zhang, F.P. Wang, X.D. Wang, Electroanalysis 18 (2006) 2475.
[29] (a) L. Cheng, J.A. Cox, Chem. Mater. 14 (2002) 6;
(b) L.H. Bi, H.Y. Wang, Y. Shen, E.K. Wang, S.J. Dong, Electrochem. Commun. 5 (2003) 913.
[30] (a) T.R. Zhang, S.Q. Liu, D.G. Kurth, C.F.J. Faul, Adv. Func. Mater. 19 (2009) 642;
(b) S.Q. Liu, H. Mohwald, D. Volkmer, D.G. Kurth, Langmuir 22 (2006) 1949;
(c) M. Jiang, X.D. Zhai, M.H. Liu, Langmuir 21 (2005) 11128;
(d) B.B. Xu, L. Xu, G.G. Gao, Y.B. Yang, W.H. Guo, S.P. Liu, Z.Z. Sun, Electrochim. Acta 54 (2009) 2246.
[31] (a) B. Wang, L.H. Bi, L.X. Wu, J. Mater. Chem. 21 (2011) 69;
(b) B. Wang, Z.D. Yin, L.H. Bi, L.X. Wu, Chem. Commun. 46 (2010) 7163.
[32] S.Q. Liu, D.G. Kurth, D. Volkmer, Chem. Commun. 9 (2002) 976.
[33] (a) G. Charron, A. Giusti, S. Mazerat, P. Mialane, A. Gloter, F. Miserque, B. Keita, L. Nadjo, A. Filoramo, E. Riviere, W. Wernsdorfer, V. Huc, J.P. Bourgoin, T. Mallah, Nanoscale 2 (2010) 139;
(b) W.H. Guo, L. Xu, F.Y. Li, B.B. Xu, Y.B. Yang, S.P. Liu, Z.X. Sun, Electrochim. Acta 55 (2010) 1523.
[34] M.H. Huang, L.H. Bi, Y. Shen, B.F. Liu, S.J. Dong, J. Phys. Chem. B. 112 (2004) 9780.
[35] Z.X. Sun, L. Xu, W.H. Guo, B.B. Xu, S.P. Liu, F.Y. Li, J. Phys. Chem. C. 114 (2010) 5211.
[36] C.X. Li, K.P. O'Halloran, H.Y. Ma, S.L. Shi, J. Phys. Chem. B. 113 (2009) 8043.
[37] J. Kim, L. Lee, B.K. Niece, J.X. Wang, A.A. Gewirth, J. Phys. Chem. B. 108 (2004) 7927.
[38] B. Qin, H.Y. Chen, H. Liang, L. Fu, X.F. Liu, X.H. Qiu, S.Q. Liu, R. Song, Z.Y. Tang, J. Am. Chem. Soc. 132 (2010) 2886.
[39] (a) Z. Ma, Q. Liu, Z.M. Cui, S.W. Bian, W.G. Song, J. Phys. Chem. C. 112 (2008) 8875;
(b) H.Z. Huang, Q. Yuan, X.R. Yang, Colloids Surf. B 39 (2004) 31.
[40] L.H. Bi, W.H. Zhou, J.G. Jiang, S.J. Dong, J. Electroanal. Chem. 624 (2008) 269.
[41] Y.G. Sun, Y.N. Xia, Science 298 (2002) 2176.

[42] S. Navaladian, C.M. Janet, B. Viswanathan, T.K. Varadarajan, R.P. Viswanath, J. Phys. Chem. C. 111 (2007) 14150.
[43] H. Borchert, E.V. Shevehenko, A. Robert, I. Mekis, A. Kornowski, G. Grubel, H. Weller, Langmuir 21 (2005) 1931.
[44] S. Link, M.A. El-Sayed, J. Phys. Chem. B. 103 (1999) 4212.
[45] T. Sawitowski, Y. Miquel, A. Heilmann, G. Schmid, Adv. Func. Mater. 11 (2001) 435.
[46] K. Lance Kelly, E. Coronado, L. Lin Zhao, G.C. Schatz, J. Phys. Chem. B. 107 (2003) 668.
[47] B. Lim, P.H.C. Camargo, Y. Xia, Langmuir 24 (2008) 10437.
[48] Y.F. Wang, A. Neyman, E. Arkhangelsky, V. Gitis, L. Meshi, I.A. Weinstock, J. Am. Chem. Soc. 131 (2009) 17412.
[49] Y. Yan, B. Li, W. Li, H.L. Li, L.X. Wu, Soft Matter 20 (2009) 4047.
[50] Y.Y. Bao, L.H. Bi, L.X. Wu, S.S. Mal, U. Kortz, Langmuir 25 (2009) 13000.